Investigation of the inhibitory activity of some dietary bioactive flavonoids against SARS-CoV-2 using molecular dynamics simulations and MM-PBSA calculations

Jibin K. Varughese, K. L. Joseph Libin, K. S. Sindhu, A. V. Rosily & T. G. Abi

View supplementary material ↗	Published online: 23 Feb 2021.
Submit your article to this journal ↗	Article views: 198
View related articles ↗	View Crossmark data ↗
Citing articles: 3 View citing articles ↗	

Taylor & Francis
Taylor & Francis Group

Check for updates

Investigation of the inhibitory activity of some dietary bioactive flavonoids against SARS-CoV-2 using molecular dynamics simulations and MM-PBSA calculations

Jibin K. Varughese[a], K. L. Joseph Libin[a], K. S. Sindhu[b] (iD), A. V. Rosily[b] and T. G. Abi[a] (iD)

[a]Department of Chemistry, Sacred Heart College, Thevara, Kochi, Kerala, India; [b]Department of Chemistry, Morning Star Home Science College Angamaly, Kerala, India

Communicated by Ramaswamy H. Sarma

ABSTRACT

Eventhough the development of vaccine against COVID-19 pandemic is progressing in different part of the world a well-defined treatment plan is not yet developed. Therefore, we investigate the inhibitory activity of a group of dietary bioactive flavonoids against SARS-CoV-2 main protease (M^{pro}), which are identified as one of the potential targets in the drug discovery process of COVID-19. After the initial virtual screening of a number of bioactive flavonoids, the binding affinity of three compounds - Naringin, Naringenin and Amentoflavone - at the active site of M^{pro} was investigated through MD Simulations, MM-PBSA and DFT Binding Energy calculations. From the MD trajectory analysis, Amentoflavone and Naringin showed consistent protein-ligand interactions with the aminoacid residues of the active site domains of M^{pro}. The excellent inhibitory activity of Amentoflavone and Naringin was established from its MM-PBSA binding energy values of -190.50 and $-129.87\,kJ/mol$ respectively. The MET165 residue of M^{pro} is identified as one of the key residue which contributed significantly to MM-PBSA binding energy through hydrophobic interactions. Furthermore, the DFT binding energy values of Amentoflavone (-182.92 kJ/mol) and Naringin (-160.67 kJ/mol) in active site molecular clusters with hydrogen bonds confirmed their potential inhibitory activity. These compounds are of high interest because of their wide availability, low cost, no side effects, and long history of use. We can prevent the severity of this disease for home care patients using these effective dietary supplements. We are hopeful that our results have implications for the development of prophylaxis of COVID-19.

1. Introduction

After the first case of coronavirus pandemic (COVID-19) was reported from China during the last week of December 2019 (Wu et al., 2020; Zhou et al., 2020), it has killed thousands of people worldwide, and even after stringent containment measures, the spread of the virus over the globe is increasing day by day. One hundred and four million people were affected worldwide, and more than 2 million have been killed so far. (data from https://www.worldometers.info/coronavirus/ on 3rd February 2021). This spotlights the importance of discovering and developing effective drugs at the earliest.

The root cause of COVID-19 is SARS-CoV-2, a member of the beta coronavirus with a single-stranded RNA (Chan et al., 2020). The encoded SARS-CoV-2 genomic structure shows that it contains four major structural proteins: the spike (S) protein, nucleocapsid (N) protein, membrane (M) protein, and the envelope (E) protein (Schoeman & Fielding, 2019). The S protein is responsible for the target cell entry by utilizing the host cell receptor, Angiotensin-Converting Enzyme2 (ACE-2) (Li et al., 2003). Attachment of S protein to the ACE2

receptor is activated by a transmembrane serine protease, TMPRSS2 (Iwata-Yoshikawa et al., 2019). Once it enters the host cell system, RNA of the virus is released, undergoing replication and finally converted into an effector protein by virus proteases. In the whole process, the main protease (M^{pro}) of SARS-CoV-2 is identified as the crucial component for viral replication and transcription. So researchers believe that strategies which can target M^{pro} can prevent pandemic COVID-19 to a great extent (Jin et al., 2020; 2020)

A specific antiviral drug against SARS-CoV-2 is yet to be discovered and several attempts are being made to develop a potential drug. As the time for clinical trials gets longer the number of fatalities also rises. In this context, one strategy is to repurpose antiviral drugs. The effectiveness of repurposing of antiviral drugs (Saha et al., 2020) in the treatment of the disease is extensively studied across the globe. Among those drugs, Remdesivir (Grein et al., 2020) and Hydroxychloroquine (Yao et al., 2020) are widely used in emergencies. Various researchers have pointed to the applicability of drugs like Tocilizumab (Cortegiani et al., 2021), Teicoplanin (Zhang et al., 2020), Carfilzomib (Wang, 2020), Baricitinib (Richardson et al.,

2020), Ivermectin (Caly et al., 2020), Lopinavir and Ritonavir (Chu et al., 2004) and many more, but most of them found to have only moderate anti-SARS-CoV-2 activity and sometimes side effects are also reported (Jomah et al., 2020). Several spices, phytochemicals and traditional medicines are also found to have some inhibitory effect on the protease of SARS-CoV-2 in virtual and compound library screening (Ibrahim et al., 2020; Idrees et al., 2020; Mani et al., 2020) Myricitrin (Joshi et al., 2020), Leucoefdin (Singh & Mishra, 2020), natural poly phenols (Ghosh et al., 2020; 2020), Terpenes (Muhseen et al., 2020), Carnosol and Rosmanol (Umesh et al., 2020), etc., are some of the reported phytochemicals which show better binding affinity towards target protein. The vaccine safety trials against the pandemic are also going on since March 2020. There were around 234 vaccine candidates from 165 countries, and only a few of them were reached the last phase of trials. However, the efficiency of a single vaccine is doubtful due to the rapid change of the target protein's functional nature. Thus, even though some promising results have achieved so far, a perfect treatment for COVID-19 may still take a longer time to be developed.

The patients with severe COVID-19 symptoms should be treated with well-established pharmacological agents recommended by WHO based on disease severity. However, in this present scenario where hospitalization may not be possible for all the patients, the burden on the health care system all over the world increases. WHO recommended safe home care for patients with mild symptoms and without underlying chronic conditions such as lung or heart disease and renal failure. Moreover, in most countries, people with mild symptoms are kept in their homes (Gandhi et al., 2020). This figure out the importance of dietary bioactive compounds that can protect or diminish this disease's severity without adverse side effects.

It will be highly appreciable if we can make dietary recommendations or practice of using bioactive compounds for anti COVID-19 treatment. Dietary bioactive compounds (Dietary Bioactive Components, 2018) such as flavonoids, isothiocyanates, carotenoids, anthocyanins, etc., are extra nutritional constituents that typically occur in small quantities in fruits, vegetables, whole grains, legumes, oils, and nuts. Most of them have beneficial health effects and are widely utilized to treat both lifestyle and chronic diseases (Liu, 2013). Previous studies associated with the use of flavonoids as potential drugs for cancer, obesity, hypertension, and other diseases are available (Middleton et al., 2000; Scalbert et al., 2005). The reports of flavonoids as potential antiviral compounds (Dai et al., 2019; Moghaddam et al., 2014) are also available in the literature. A recent study on computer-guided identification of citrus flavonoids highlights the use of Taxifolin as an inhibitor of SARS-CoV-2 (Gogoi et al., 2020).

To initialize the drug design process, we performed the virtual screening of some dietary bioactive compounds based on molecular Docking towards the binding site of M^{pro} (PDB ID 6LU7) where the N3 inhibitor is located. We screened various plant-based nutrients particularly flavonoids that have inhibitory activity against M^{pro}. Among these compounds,
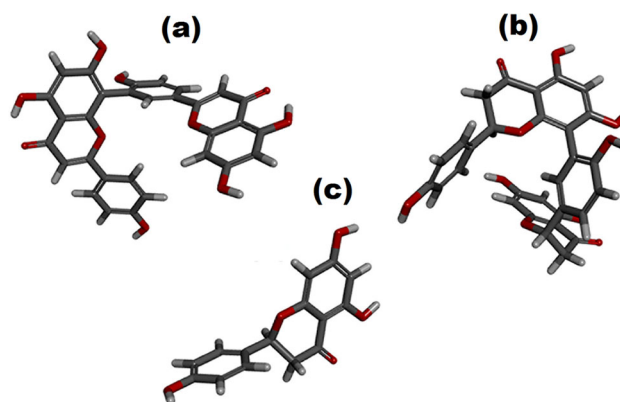

Figure 1. Optimized 3D structures of selected ligands with their Pubchem IDs (a) Amentoflavone (5281600), (b) Naringin- (442428), (c) Naringenin (932).

Naringin, Naringenin, and Amentoflavone were found to possess strong antiviral activity against the receptor.

Naringin and Naringenin are the two most important flavonoids thus far isolated from citrus fruits. These flavonoids were found to possess strong antiviral, antioxidant, and anti-inflammatory activities both in vitro and in vivo (Ahmad et al., 2015; Chen et al., 2016; Salehi et al., 2019). Even though the average daily intake of these flavonoids is not well studied, the mean intake can be estimated from tea, citrus fruits, citrus fruit juices, and wine, etc. Amentoflavone is a biflavonoid found particularly in Ginkgo biloba plant. It shows strong antiviral activity toward SARS-CoV-1 (Ryu et al., 2010), Herpes Simplex Virus type 1 (HSV-1), and Acyclovir resistant (Li et al., 2019) viruses. Interestingly, Naringin and Amentoflavone are available as nutritional supplements from different commercial sources. Hence we investigated whether these compounds could act as promising candidates against COVID-19 through molecular dynamics simulation followed by Molecular Mechanics Poisson Boltzmann Surface Area (MM-PBSA) and Density functional Theory (DFT) binding energy calculations. The best docking poses that lie in the domain of the active site of M^{pro} is exclusively used as the initial conformation for molecular dynamics studies. The MD trajectory analysis mainly focused on hydrogen bond occupancy of aminoacid residues around the ligands and we observed the formation of consistent hydrogen bonds particularly with Amentoflavone. Further, MM-PBSA and DFT binding energies confirmed the results obtained from the docking calculations.

2. Materials and methods

2.1. Molecular Docking calculations

We used the crystal structure of the protein SARS-CoV-2 (PDB ID: 6LU7) from the RCSB protein databank in the Docking calculations. Based on previous literature studies, several dietary bioactive compounds were selected, and Docking was performed. Among those compounds, we report three naturally available compounds with significant binding affinity with M^{pro}. The structure data files (SDF) of those compounds, Naringin, Naringenin, and Amentoflavone, were obtained from the Pubchem database. Further, they are subjected to geometry optimization using B3LYP/SVP (Becke, 1988; Schäfer et al.,

1992) method with Turbomole (Bauernschmitt et al., 1997) for getting a better 3D geometry for protein-ligand docking calculations. The 3D representations of the optimized structures of ligands are given in Figure 1.

The molecular docking calculations are performed using Autodock Tools and Vina Scoring functions (Trott & Olson, 2010). The initial preparation of the PDB structure is carried out by removing water and N3 inhibitor which is covalently bonded to CYS145 of M^{pro} followed by the addition of missing hydrogens and charges. Thus, the CYS145 residue in the M^{pro} is terminated using a covalently bonded hydrogen atom to S atom. The Cartesian coordinates of the binding site in Chain A of M^{pro} with 306 amino acid residues are located as x = −13.662, y = 14.927, z = 73.564. The particular location lie in the neighborhood of amino acid residues of substrate binding site as per the structural information of M^{pro} complexes with N3 inhibitor (Dai et al., 2020; Kumar et al., 2020). For docking calculations, grid box centered on the binding site coordinates are used. The total number of grid points per map is 6400 where 40 grid points each are fixed in x, y and z dimensions respectively. The grid point spacing and exhaustiveness used in the current calculation is 1 Å and 8 respectively. The best binding poses with higher binding energy are calculated and are used for further MD studies.

2.2. Molecular dynamics simulations

The conformations of the protein-ligand complex obtained from molecular docking calculations were used as the initial input for molecular dynamics simulations. GROMACS (Berendsen et al., 1995) 5.1.5 molecular dynamics package is used to execute simulations. OPLS All Atom Force Field parameters (Jorgensen et al., 1996) are used in the simulation procedure. The OPLS topology parameters for the ligands were generated from LigPargen Server (Dodda et al., 2017). The protein-ligand complex structure is neutralized with four sodium ions and solvated using SPC/E waters (Toukan & Rahman, 1985) in a cubic box with periodic boundary conditions. The solvated protein-ligand complex system was subjected to an energy minimization procedure using the steepest-descent minimization algorithm. A 1 ns simulation of NVT and NPT equilibration is preceded using the energy minimized coordinates of the solvated protein-ligand complex. The equilibrated system is further preceded to the final production run for 100 ns and 2 fs time step. The temperature of the system is maintained as 300 K using Berendsen thermostat, and the pressure of the system is maintained as 1 bar using Berendsen barostat (Berendsen et al., 1984). The computation of short-range forces of the simulating system is managed using the Verlet neighbor list and long-range electrostatic forces using the particle-mesh Ewald summation method (Di Pierro et al., 2015).

Coordinates from the trajectory were written every 10 ps to get a sufficient number of frames for analysis. RMSD analysis of the complex with respect to the backbone ensures the stability of ligands inside the active site of the protein. Exclusive mapping and analysis of hydrogen bonds between ligand and active site residues of target protein were performed using gmx_hbond tool of GROMACS and our own shell scripts. The fluctuations in the secondary structure of the protein conformation during MD simulation is monitored using DSSP analysis (Kabsch & Sander, 1983).

2.3. MM-PBSA binding free energy calculations

The binding affinity of a ligand in terms of binding free energy can be calculated using the MM-PBSA method, which is one of the most common endpoint free energy methods developed by Kollman and coworkers (Kollman et al., 2000; Wang et al., 2019) The method is commonly used to evaluate the structural stability, binding affinities, and estimate hot spots (Zoete et al., 2010). Furthermore, MM-PBSA allows the study of contributions from individual protein-ligand residues, which gives detailed residue-specific energetic contributions to the binding system and identifies dominant binding interactions (Li et al., 2019). The effective use of this method in the drug discovery process, particularly for finding inhibitors against target proteins, is popularly known with experimental validation (Genheden & Ryde, 2015). Very recent reports of MM-PBSA binding energy calculations related to inhibitors of SARS-CoV-2 are also available (Wang, 2020). The basic principles of MM-PBSA are well documented in previous studies, and we performed the calculations using g_mmpbsa code (Kumari et al., 2014). We utilized a single trajectory approach to obtain the energy values associated with protein (P), ligand (L), and protein-ligand complex (C) conformations from the MD trajectory. The binding free energy of the ligand-protein complex in the solution phase is explained using Equation (1).

$$G_{bind} = G_C - (G_P + G_L) \tag{1}$$

The free energy of any individual component is given by

$$G = E_{MM} + G_{solv} - TS$$
$$E_{MM} = E_{bonded} + E_{elec} + E_{vdW} \tag{2}$$

The (E_{MM}) term in Equation (2) is the energy of molecular mechanics (MM) potential with bonding and non-bonding (van der Waals + electrostatic) terms. As we assume that the bound and unbound forms of protein and ligand conformations in the single trajectory method are similar, the value of E_{bonded} energy can be taken as zero. The conformational entropy term (TS) associated with complex and isolated protein is calculated in the vacuum environment. In the current methodology, we focused on the contribution of individual residues of protein and ligands to the individual components of E_{MM} and G_{solv} terms given in Equations (2, 3, and 4) instead of considering absolute binding free energy. The term TS is ignored in this study as the change of this term does not affect the relative binding energy of ligands (Hou & Zhang, 2020).

$$G_{solv} = G_{PB} + G_{SA} \tag{3}$$
$$G_{SA} = \gamma_{SASA} + b \tag{4}$$

The free energy of solvation (G_{solv}) in Equation (3) is calculated as the sum of the non-linearized version of the
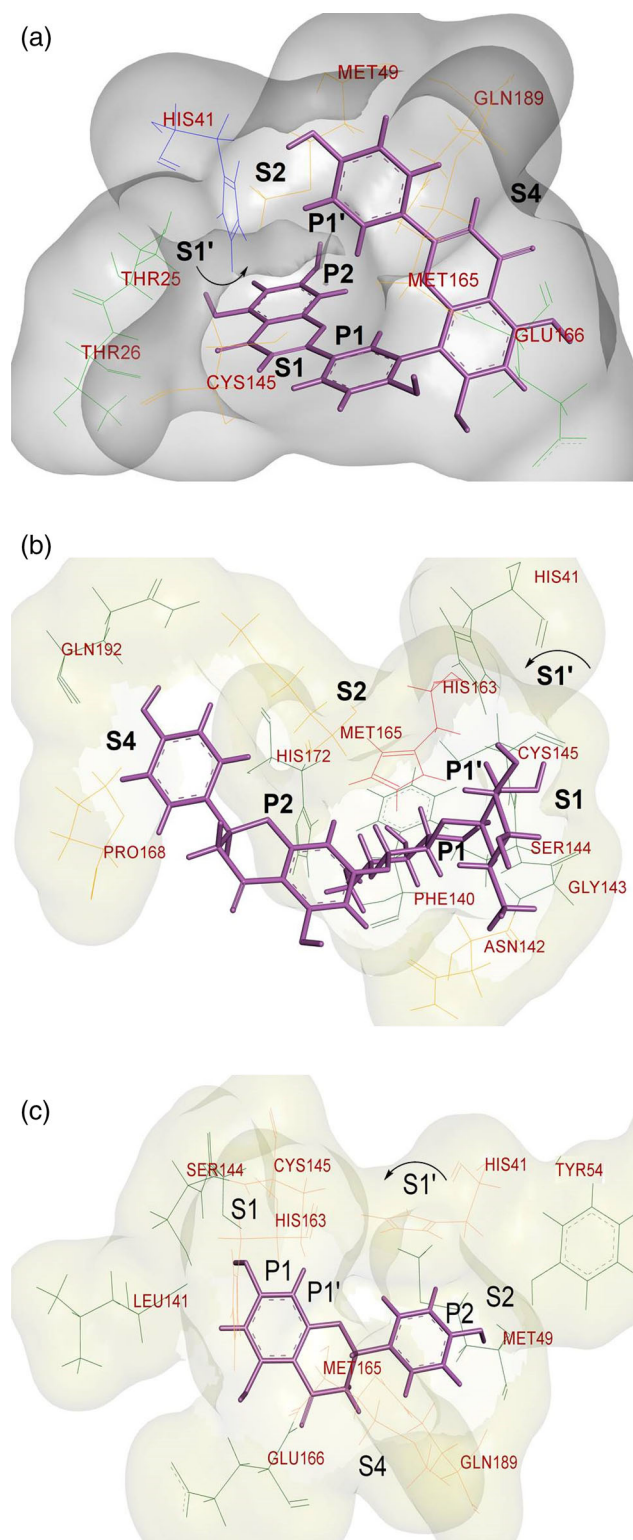
Figure 2. a: A 3D surface representation of best docking pose of Amentoflavone at the active site of M^{pro}. The amino acid residues that form Hydrogen bonds (HB), Hydrophobic-van der Waal (HP-vdW) contacts and both HB/HP-vdW interactions are depicted using green, yellow and blue colored lines respectively. The active subsites (S1, S1', S2, S4) and their associated ligand pockets (P1, P1', P2) are also shown. b: A 3D surface representation of best docking pose of Naringin at the active site of M^{pro}. The amino acid residues that form Hydrogen bonds (HB), Hydrophobic-van der Waal (HP-vdW) contacts and unfavorable interactions are depicted using green, yellow and red colored lines respectively. c: A 3D surface representation of best docking pose of Naringenin at the active site of M^{pro}. The amino acid residues that form Hydrogen bonds (HB) and Hydrophobic-van der Waal (HP-vdW) contacts are depicted using green and yellow colored lines respectively.

Poisson-Boltzmann Equation (G_{PB}) that gives the energy of polar interactions. The nonpolar energy (G_{SA}) term is estimated using the solvent-accessible surface area (SASA). In Equation (4), the γ term is a coefficient related to the surface tension of the solvent, and b is the fitting parameter. The values of dielectric constants used for solvent, solute, and vacuum in the g_mmpbsa calculations are 80, 2, and 1, respectively, and the solvent probe radius is 1.4 Å. We have carried out twenty sets of calculations by utilizing 50 snapshots at regular intervals of 20 ps taken from the frames of each 1 ns trajectory between 81-100 ns. The studies of energy decomposition per residues that contributed to the reported MM-PBSA binding energy of ligand in the protein-ligand complex are also performed.

2.4. DFT Binding energy calculation

We have calculated the binding energy with DFT calculations on the active site cluster molecules containing the ligand and the amino acid residues that have hydrogen-bonding interactions with the ligand. The MD trajectory sampling and hydrogen bond occupancy analysis show that an average of 3-4 bonds is formed around the ligands (Amentoflavone and Naringin) during MD simulation. We identified three such amino acid residues of M^{pro} which form consistent hydrogen bonds around Amentoflavone and Naringin on the basis of higher occupancy percentage. We avoided more amino acid residues (with hydrophobic contacts) that lie farther than hydrogen bonded residues as their incorporation may affect the accuracy of DFT (quantum calculation) results. We extracted a representative frame of the ligand with three hydrogen-bonded residues from the trajectory. The ligand, the residues, and the ligand complex with three hydrogen-bonded residues are denoted as (LIG), (RES), and (LIG-RES), respectively. The assigned reaction associated with the procedure is given as

$$(LIG) + (RES) \rightarrow (LIG - RES) \quad (5)$$
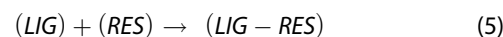
The conformations associated with each species are subjected to gaseous phase geometry optimization followed by single-point energy calculations using the B3LYP/SVP (Becke, 1988; Schäfer et al., 1992) method in Turbomole software. The binding energy (BE) of the ligand with hydrogen-bonded residues is given by Equation (6).

$$BE = E(RES - LIG) - E\big[(RES) + (LIG)\big] \quad (6)$$

3 Result and discussion

3.1. Molecular Docking studies

We screened various flavonoids against M^{pro} and their docking scores are provided in the supporting Information. The docking scores of the three selected ligands, Amentoflavone (-9.6 kcal/mol), Naringin (-8.3 kcal/mol), and Naringenin (-7.8 kcal/mol) with M^{pro} obtained from molecular docking calculations and ligand-protein non-bonding interactions analyzed using PLIP tool (Salentin et al., 2015) are represented in Figure 2.
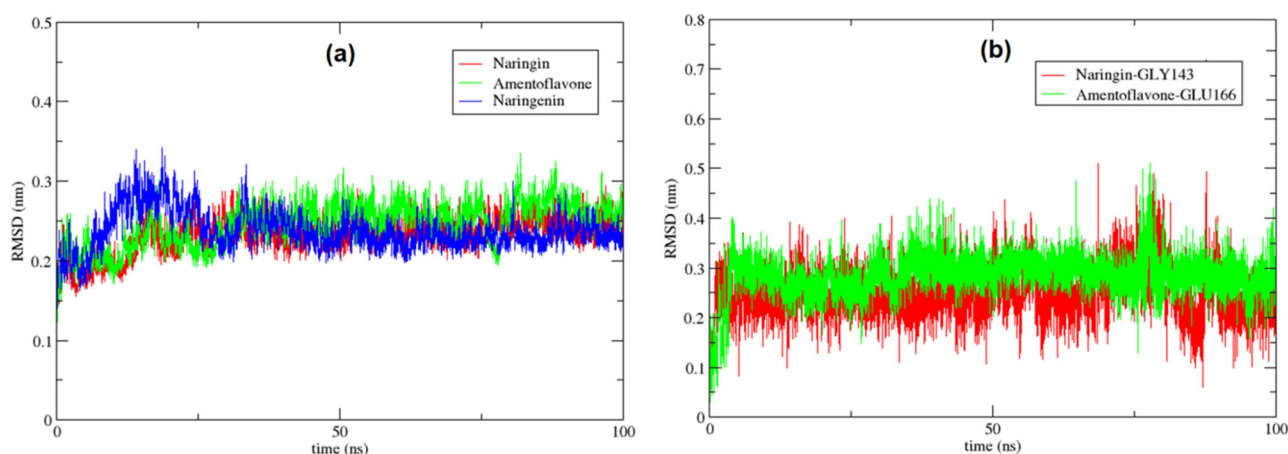
Figure 3. RMSD plots of (a) complex with respect to backbone and (b) residue atoms with respect to ligands.
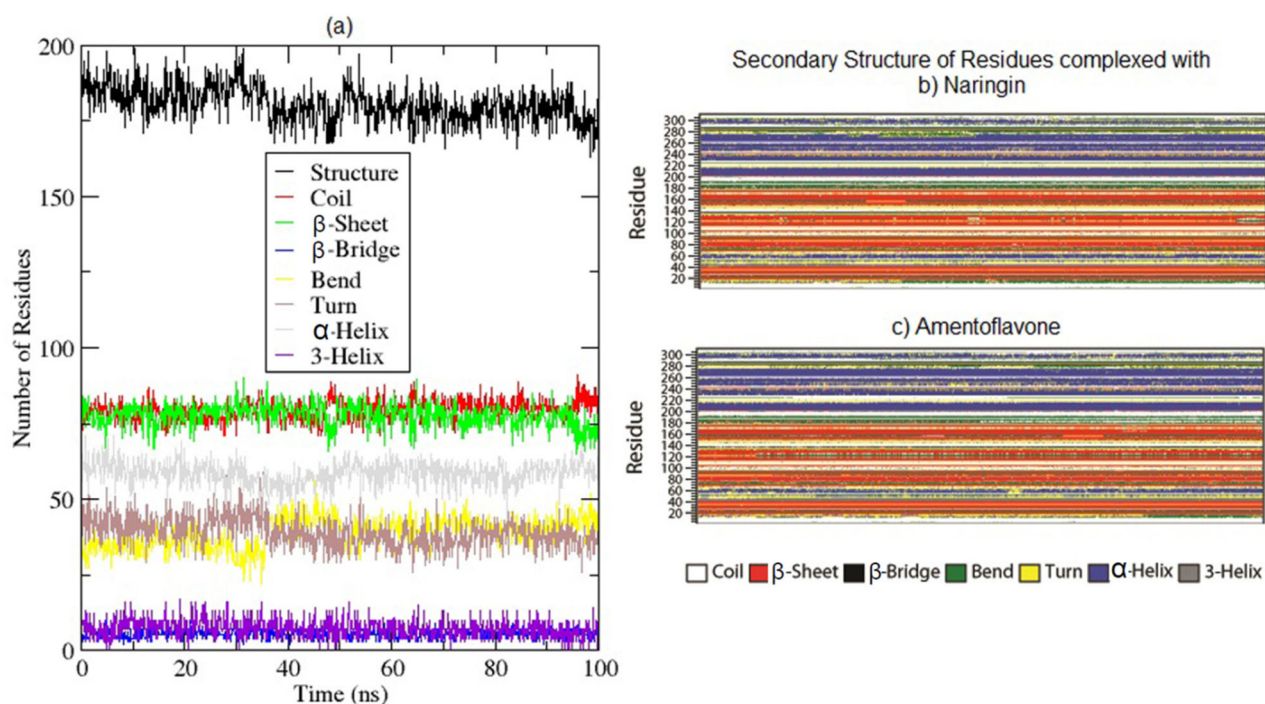

Figure 4. a) Number of residues associated with each region of secondary structure of protein in Naringin complex. DSSP Analysis of protein structure of Naringin complex (b) and Amentoflavone complex (c) during the course of the simulation.

Furthermore, the characteristics of best docking poses for the selected ligands and their binding pockets are analyzed by comparing them with the binding mode of N3 inhibitor in the active site domains S1, S1' S2 and S4 (Jin et al., 2020) respectively. These domains and the corresponding residues in the binding pocket of the ligands (P1, P1', P2) are depicted as a surface representation in Figure 2. Amentoflavone has both hydrophobic and hydrogen bond interactions with HIS41 residue at P1' moiety. The major portion of the ligand structure lies in the P2 residues (MET49 and MET165) of M^{pro} with strong hydrophobic interactions (Figure 2a). The P1 position of the ligand is accommodated by CYS145 residue with a hydrophobic interaction. However, any covalent bond of CYS145 residue with Amentoflavone is not observed here on comparison with N3-M^{pro} complex as the S atom of CYS145 is terminated using covalently bonded hydrogen atom.

Moreover, Amentoflavone possesses hydrogen bonding interactions with THR25, THR26, GLU166 and hydrophobic contact with GLN189 of the active site regions. The significant hydrophobic interactions augmented its docking score to −9.6 kcal/mol. The P1 residues (CYS145, GLY143 and SER144) and P1' residue (HIS41) forms hydrogen bonds with Naringin. The other hydrogen bonded residues in the binding pockets of the ligand are PHE140, HIS172 and GLN192 respectively (Figure 2b). Naringin has hydrophobic contact with MET165 of P2 region along with ASN142 and PRO168 residues. However, one unfavourable interaction of HIS163 residue with steric repulsion is observed here which might be the reason for the moderate binding score (-8.3 kcal/mol) irrespective of its higher number of hydrogen bonds and hydrophobic contacts. Ten amino acid residues that belong to the four binding subsites of M^{pro} interact with Naringenin
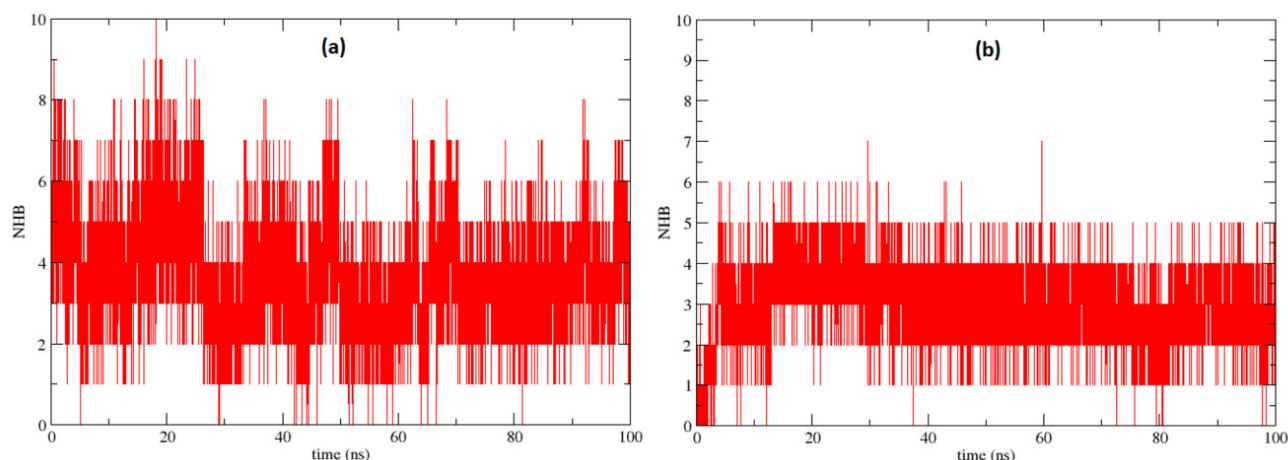
Figure 5. Number of hydrogen bonds formed by (a) Naringin and (b) Amentoflavone.

through hydrogen bonds or hydrophobic contacts. The active amino acid residues associated with the binding pockets of the ligands discussed here resemble the binding sites of reported N3-M^{pro} complex. Thus, these docking poses could be the right choice for initial conformations in molecular dynamics studies. The validations of docking results are further done using Autodock 4.2.6, and the results are provided in the supporting information.

3.2. MD Trajectory analysis

The conformation obtained from the docking studies with the best binding pose is solvated, minimized and subjected to further MD simulation studies. During the MD run, the equilibration is monitored by observing the steady energies of the system with respect to time. RMSD's of the complex fitting to the backbone indicates the stability of the complex in a solvated system (Figure 3a). The structure of all protein-ligand complexes was found to be stabilized within 0.2 nm from the backbone. Then, we extracted the active site residues with more residence time around the ligand by hydrogen bond occupancy calculations of the MD trajectory. The RMSD's of the residues GLY143(NH) and GLU166(NH) are fitted against corresponding ligands, Naringin, and Amentoflavone, respectively, as shown in Figure (3b). The stabilization of residues at a distance of 0.15-0.3 nm is clear evidence of non-bonding interactions between the residues and the ligands.

Even though larger time scale MD simulations are needed, fluctuations in the secondary structure of protein can also be mapped from the 100 ns MD trajectory. DSSP analysis (Figure 4) and Ramachandran plot analysis are utilized for this purpose. Out of 306 residues of M^{pro}, an average of 58, 76.5, 79.6, and 40 residues constantly retain in alpha helix, beta-sheet, coils, and turns regions of the secondary structure of M^{pro} complexed with Naringin (Figure 4a). Similar results are observed for Amentoflavone complexed with M^{pro}. Moreover, the continuity of the color code for alpha-helical region, beta-sheet, and turns are observed throughout the simulations (Figure 4b and c). This indicates that most of the amino acid residues of the M^{pro} retained their position during complex formation with the ligands. Presence of higher percentage of residues in the favored/allowed regions of the

Ramachandran plot confirmed the conservation of the secondary protein structure.

3.3. Hydrogen bond occupancy analysis

We have carried out an extensive hydrogen bond occupancy analysis between M^{pro} and the ligands using the MD trajectories. This could provide deeper insights into the hydrogen bond interaction between the active site residues and ligands. The hydrogen bond criteria of gmx_hbond tool are used as the standard parameter for extracting hydrogen bonds from the MD trajectory. The hydrogen bond distance is fixed as ≤ 3.5 Å (0.35 nm) and angle between donor-hydrogen-acceptor should be $180°\pm30°$. We analyzed the number of hydrogen bonds (NHB) formed between protein residues and ligands by utilizing 10000 frames at 10 ps intervals and found an average of 3.8, 3.0, and 0.8 hydrogen bonds formed by Naringin (Figure 5a), Amentoflavone (Figure 5b) and Naringenin respectively.

Then we identified the consistent hydrogen bond pairs between the residues and ligands having a total occupancy $> 50\%$ (Table 1). GLU166 and HIS41 formed hydrogen bonds with Amentoflavone and GLY143 with Naringin through two donor/acceptor atoms. Further, the percentage occupancy of a particular hydrogen-bond at regular intervals of 100 ps, starting from 0 ns up to 100 ns, is calculated to plot the hydrogen bond occupancy autocorrelation function $OP(t)$. The percentage occupancy of a particular bond from 0 to 0.1 ns is taken as $HB(t_0)$ and successive occupancies as $HB(t)$. Using these values, $OP(t)$ is calculated for specific hydrogen bond pairs (Equation (7)), a measure of the lifetime of a particular hydrogen-bonded pair. The denominator is the normalization factor with the square of 100 percent occupancy of the hydrogen bond.

$$OP(t) = \frac{\langle HB(t_0)HB(t)\rangle}{100^2} \tag{7}$$

The estimated order of strength of hydrogen bonds formed by the residues based on this calculation is given as GLY143 > HIS163 > GLN192 > SER144 for Naringin (Figure 6a) and GLU166 > HIS41 > CYS44 for Amentoflavone (Figure 6b). The stability of hydrogen bonds of top hit residues GLY143

Table 1. Hydrogen bond occupancy of ligands with M^pro.

Ligand (Residue-LIG307)	Protein Residue	Hydrogen Bond (Donor-Acceptor)	Percentage of Total Occupancy
Amentoflavone	GLU166	GLU166@N – LIG307@O0W LIG307@O0W – GLU166@OE2	96.8
	CYS44	LIG307@O1H – CYS44@O	85.1
	HIS41	LIG307@O01 – HIS41@ND1 LIG307@O01 – HIS41@NE2	65.0
Naringin	GLY143	GLY143@N-LIG307@O07 GLY143@N-LIG307@O09	98.3
	HIS163	HIS163@NE2-LIG307@O0C	62.5
	GLN192	GLN192@NE2-LIG307@O00	54.2
	SER144	SER144@OG-:2231-LIG307@O09	51.5

with Naringin and GLU166 with Amentoflavone has been already confirmed from the RMSD plots (Figure 3b). One interesting observation is, although on average, more numbers of hydrogen bonds are formed around Naringin, consistent hydrogen bond pairs are formed around Amentoflavone.

Other amino acid residues that show moderate or weak hydrogen bonding interactions with the ligands in terms of total hydrogen bond occupancies are also analyzed. The occupancy percentage of hydrogen bonds formed by GLN189, HIS163, THR190, and ASP187 with Amentoflavone is 48.0, 43.5, 24.3, and 12.0, respectively. In comparison, the hydrogen bond occupancies of residues such as ASN142, GLN189, CYS145, and GLU166 with Naringin are 47.6, 44.0, 11.6, and 11.5, respectively. These studies also validate the existence of various hydrogen bonding interactions (Frecer & Miertus, 2020) between GLY143, GLN192, SER144, and HIS163 residues with Naringin (Figure 2b) and GLU166, HIS41 residues with Amentoflavone (Figure 2c) obtained from the docking studies. ASN142 and GLY143 show weak hydrogen bonding interactions with occupancy of 25.5 and 23.2 percentages, respectively, with Naringenin, is not plotted here. Based on hydrogen bond occupancy analysis, we can rank the binding affinity of ligands in the order Amentoflavone > Naringin > Naringenin with M^pro. Thus, Amentoflavone and Naringin have a better binding propensity, which confers their capacity to act as better inhibitors.

3.4. Structure and contact map analysis from MD replicates

We extended the contact map (hydrogen bond) analysis between protein-ligand residues to other non-bonding interactions by performing multiple replicate long scale molecular dynamics simulations. To reduce the nondeterministic nature of protein and ligand conformations, we carefully did a series of redocking calculations using the sampling of conformations from the above-reported MD trajectory. For this purpose, we extracted protein-ligand conformations taken from snapshots between 80-100 ns of the reported MD trajectory for Amentoflavone and Naringin complexed with M^pro. We then separated the protein and ligand structures from each snapshot and repeated the same docking procedure explained in 2.1. The initial conformation for doing the multiple replicate simulations was chosen from the selected redocking poses with more similarity with the pose used for the reported MD simulation. We performed five replicate

100 ns MD simulations in the case of Naringin and Amentoflavone each. Further, we extended these calculations to a second set of five MD replicates of 20 ns length by utilizing the conformations of 100 ns MD replicates. Thus, we performed altogether 10 replicate simulations for each ligand.

The equilibration of all replicate simulations is observed from its minimum fluctuations of potential energies, the radius of gyration, and RMSD with respect to time. As significant binding interactions were not observed in the Naringenin complex, we have not attempted its replicate simulation. The protein-ligand non-bonding interaction profile of hydrogen bonds and all types of hydrophobic-van der Waal (vdW) interactions was prepared using GROMACS tools, shell scripts, and "Discovery Studio Visualizer Software, Version 4.5". The occupancy percentage of interactions in the reported MD trajectory and an average of all replicated MD trajectories are depicted in Figure 7 (a,c) and Figure 7 (b, d) respectively. From Figure 7 (a,b), it is evident that the hydrogen bond occupancy profile of reported simulations for Amentoflavone is almost reproduced in the replicated simulations. The amino acid residues that form hydrogen bonds with Amentoflavone in the reported simulation were the same in the replicated MD trajectories.

GLU166 (> 90%) and HIS41 (above >65%) form consistent hydrogen bonds in both reported and replicated simulations. However, the hydrogen bond occupancy of CYS44 reduced from 85% to 44% in replicated simulations. The other hydrogen-bonded residues of Amentoflavone show the same trends of hydrogen bond occupancy. In the Naringin complex, the hydrogen-bonded residues and their occupancy percentage varied moderately in reported and replicated simulations. THR25, PHE294, and HIS41 show hydrogen bond occupancy of 65, 52, and 25%, respectively, in replicated simulations. GLY143, HIS163, GLN192, and SER144 show consistent hydrogen bond formation in reported and replicated simulations. It is well known that hydrophobic-vdW interactions are the key interactions for effective protein-ligand binding than hydrogen-bonding interactions. We included pi stacking, pi-cation, pi-alkyl, pi-amide, and other vdW interactions to the broad category of hydrophobic-vdW interactions (Figure 7) with a fixed bond distance range of $3.5 - 4.2$ Å (Ferreira de Freitas & Schapira, 2017). MET165 is the key hydrophobic residue that is involved in non-bonding interactions with Amentoflavone throughout and having percentage occupancy of 89 and 83 in reported and replicated simulations, respectively. Based on the profile, the order of strength of
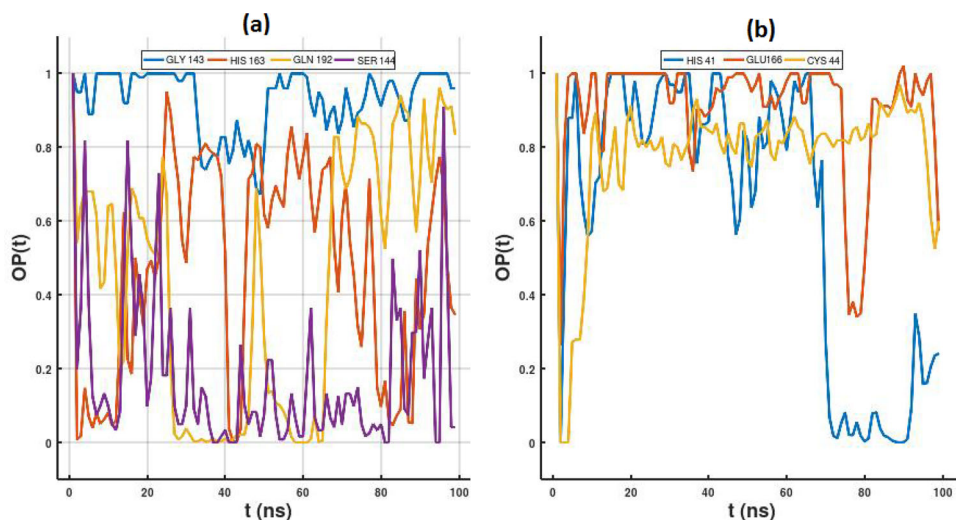
Figure 6. The hydrogen bond occupancy autocorrelation function OP(t) of specific hydrogen bond pairs of (a)Naringin (b) Amentoflavone.
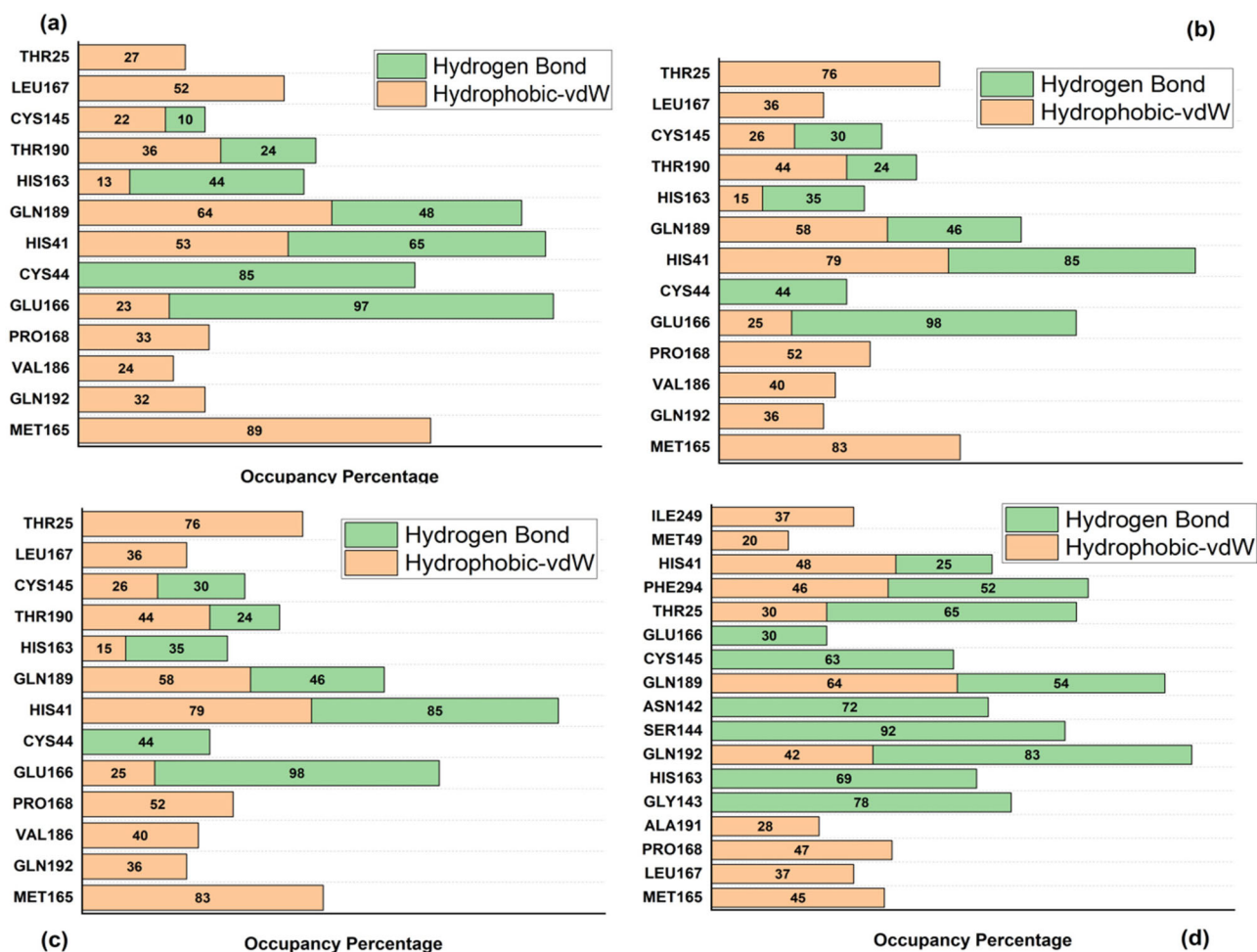

Figure 7. Protein-ligand Nonbonding interaction profile from the a) reported and b) replicated MD trajectories of Amentoflavone complex c) reported and d) replicated MD trajectories of Naringin complex.

amino acid residues that involve in the significant hydrophobic interactions with Amentoflavone in reported/replicated simulations are MET165> HIS41 > GLN189 > THR25 > LEU167 > PRO168 > THR190 > GLN192 >VAL186. The type of hydrophobic-vdW interactions in these residues are found to be pi-alkyl (MET155, PRO168), pi-pi T shaped (HIS41), pi-amide interactions

(GLN, THR), and other vdW (LEU167, VAL186), respectively. The significant residues that contributed to hydrophobic interactions with Naringin ligand are in the order GLN189 >MET165 > HIS41 > GLN192 > PRO168 > PHE294 > LEU167 >MET49 >ILE249. Among these residues, MET165, HIS41, PRO168, and PHE294 interact with the ligand through pi-

Table 2. Binding energy values and individual component energy calculated with MM-PBSA method for ligands. All reported energy values have a standard deviation within the range of 9 kJ/mol.

Ligand	van der Waal energy (kJ/mole)	Electrostatic energy (kJ/mole)	Polar solvation energy (kJ/mole)	SASA energy(Nonpolar Solvation) (kJ/mole)	Binding energy (kJ/mole)	Energy Contribution by Ligand (kJ/mol)
Amentoflavone	−255.175	−52.173	140.529	−23.683	−190.502 +/− 8.432	−101.16
Naringin	−210.240	−51.290	154.579	−22.920	−129.871+/− 8.862	−67.65
Naringenin	−128.971	−16.572	74.445	−13.471	−84.569 +/− 6.62	−42.45
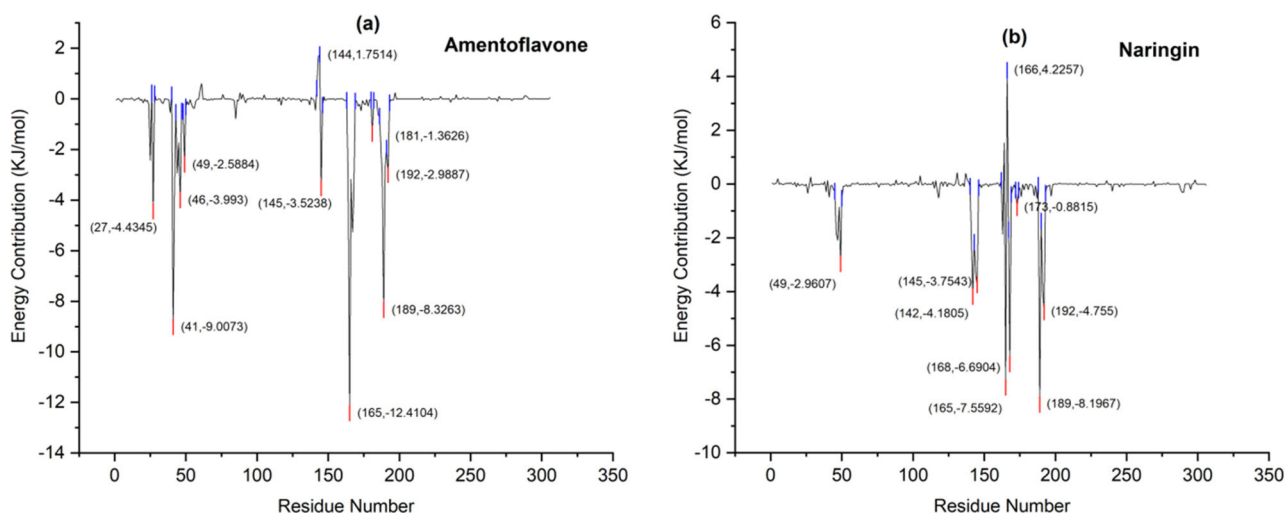
Figure 8. MM-PBSA Binding Energy decomposition of M^{pro} residues in (a) Amentoflavone complex and (b)Naringin complex.

alkyl interactions. MET49 interacts via alkyl interactions, and all other residues, including GLN189, interact through other vdW contacts. GLU166, HIS41, GLN189, HIS163, THR190 and CYS145 residues exhibit both hydrogen bonding and hydrophobic contacts with Amentoflavone in all MD trajectories. GLN189 and GLN192 residues show the similar interactions with Naringin.

3.5. Binding energy calculation using MM-PBSA method

A detailed analysis of MM-PBSA results was carried out in this section. The values of binding energy and its subsequent components from twenty sets of calculations utilize the 80-100 ns of the reported MD trajectory. Each set of calculations is performed by utilizing 50 snapshots from one ns each. We reported here [Table 2] the result from a typical set of calculations, which gives the mean value of the whole set of calculations.

The results showed that Amentoflavone possessed the highest negative binding free energy value of −190.5 kJ/mol compared to Naringin(-129.9 kJ/mol). By utilizing the energy decomposition analysis tool of g_mmpbsa, it is evident that the obtained MM-PBSA binding energy for a particular protein-ligand complex is the sum of energies contributed by all residues including the ligand residue. The energy contribution of ligand residue is −101.1 kJ/mol and −67.7 kJ/mol for Amentoflavone and Naringin respectively. The bigger energy contribution of the Amentoflavone ligand to MM-PBSA binding energy shows its excellent binding affinity towards the active site of M^{pro}. Among the individual components that contribute to the total

negative binding energy value (Table 2), the vdW energy contributes significantly to Amentoflavone and Naringin. Next to vdW energy, Electrostatic (ESE) interactions or hydrogen bonding interactions contribute to the total binding energy with negative energy values. However, those residues with unfavorable interactions with solvent molecules increase the polar solvation energy (PSE) to more positive and try to reduce the effect of energy contributions from the electrostatic part. The nonpolar solvation energy (SASA energy) term also contribute to the binding energy with negative values.

We performed MM-PBSA protein residue free energy decomposition analysis (Figure 8 and 9) for all complexes and identified the amino acid residues with significant interactions with the ligand. Those amino acid residues contributed to the MM-PBSA binding energy with negative energy values, and positive energy values are identified as hot spot and bad contact residues, respectively in energy decomposition analysis (Figure 9). In case of Amentoflavone complexed with M^{pro}, the hot spot residues with negative binding energies are MET165 (-12.4), HIS41(-9.0), GLN189(-8.3), LEU27(-4.4), CYS145(-3.5), SER46(-3.99), GLN192(-2.99), MET49(-2.59) and PHE181(-1.36) respectively. As per the evidence from the contact map analysis (Figure 7), MET165, LEU27, GLN192, and MET49 contributed significantly to the protein-ligand binding through hydrophobic interaction. The pi-alkyl interaction (hydrophobic-vdW) of MET-165 residue with Amentoflavone is more crucial in the protein-ligand complex formation. At the same time, HIS41 (-9.0), GLN189(-8.3), and CYS145(-3.5) are involved in hydrophobic as well as hydrogen bonding
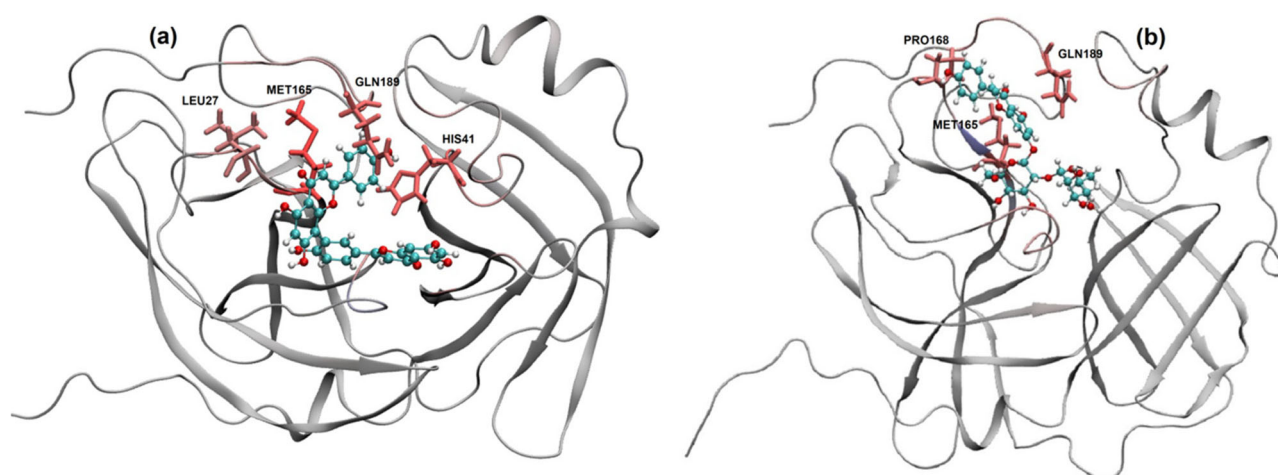
Figure 9. Hot spot residues are highlighted in Red colored licorice representation in (a) Amentoflavone complex and (b) Naringin complex. The ligand structures are highlighted using CPK representation.

interactions with Amentoflavone. However, SER144 contributes a positive value of 1.75 kJ/mol, having unfavorable interactions with the ligand. Coming to the M^{pro}-Naringin complex, the residues with negative energy contribution are GLN189(-8.19), MET165(-7.56), PRO168(-6.69), GLN192(-4.76), ASN142(-4.18), CYS145(-3.75) and MET49(-2.96). It is found that GLN189, GLN192, ASN142, and CYS145 residues of M^{pro} effectively bind with Naringin through both hydrogen bonding and non-bonding interactions. Moreover, MET165(-7.56), PRO168(-6.69), and MET49 residues have contact with Naringin through hydrophobic-vdW interactions. GLU166 shows unfavorable interactions (Figure 8b) from its positive energy value (4.2 kJ/mol).

3.6. Evaluative MM-PBSA calculations from MD replicates

The MM-PBSA results obtained from the reported simulation is validated using repeated MM-PBSA calculations from 10 replicate MD simulations each for Amentoflavone and Naringin. The results of two sets of MM-PBSA calculations as an average from each replicate simulation (by utilizing 200 snapshots from 20 ns trajectory) were chosen for further analysis. This is compared with 20 sets of MM-PBSA values obtained from the reported simulation. As we performed different sets of MM-PBSA calculations in reported and replicate simulations using an independent and random selection of snapshots, correlation analysis may not give adequate insights. Instead, the range of deviation between MM-PBSA values of reported and replicated simulations can be analyzed and evaluated using a Box and WHISKER plot (Figure 10). We have calculated the values of the first quartile (Q1), second quartile (Q2 or median), third quartile (Q3), and interquartile range IQR (Q3-Q1) of MM-PBSA binding energy (BE) values. IQR value gives the measure of the difference in the distribution of a given set of MM-PBSA values. A smaller IQR value indicates a small deviation for both sets of calculations. The Q1, Q2, Q3, and IQR values for Amentoflavone in the reported simulation (Figure 10a) are −189.61, −190.35, −190.66, and 1.05, respectively. The Q1, Q2, and Q3 values of the replicated simulations (Figure 10a) are −187.85,

−190.13, and −192.32, whereas the IQR value is 4.47. The smaller deviation of IQR values (1.05, 4.47) is a clear indication of the replication of MM-PBSA reported results for Amentoflavone. The mean values of BE (Table 3) obtained from 20 sets of calculations in the reported simulations (-190.61) and replicated simulations (-190.31) are also found to be so closer.

Moreover, the standard deviation of MM-PBSA BE values in the whole set of replicated simulations is only 3.05. This evidence strongly supports the reproduction of MM-PBSA results in the multiple MD replicates for Amentoflavone. However, the deviation of IQR values of Naringin (Figure 10 b) between reported (1.59) and replicated simulations (8.3) are larger compared to Amentoflavone. Even though the mean BE energy values (Table 3) are closer in reported (-129.873) and replicated (-132.402), the standard deviation of calculations using MD replicates is found to be 4.6.

We performed the same type of statistical analysis with individual energy components of BE (Table 3). Generally, slight variations are observed for SASA energy of both ligands is in reported and replicated simulations as indicated from the standard deviation of one or less than one in all cases. vdW, ESE, and PSE of Amentoflavone complex varied moderately in replicated data with a standard deviation of 5.5, 4.8, and 6.1, respectively. Again, for the Naringin complex, a standard deviation of 13.9, 19.9, and 16.0 is observed in vdW, ESE, and polar solvation energies in the replicated simulations. The deviations are self-explanatory as the Naringin complex is involved with more number of interacting residues and with less consistent interactions (Figure 7).

The MM-PBSA BE energy decomposition of individual residues of M^{pro} is performed for all replicate simulations, and the average energy value contributed by the specific residues from all calculations are presented in Figure 11a) Amento flavone complex and b) Naringin Complex. The key residues identified in the reported simulation (Figure 8) came into the picture again in replicated simulations. Here, we analyze those residues with energy values < −5.0 kJ/mol that contributed significantly to the protein-ligand binding through electrostatic (hydrogen bonding) interactions and hydrophobic-vdW interactions. From the whole exercise of
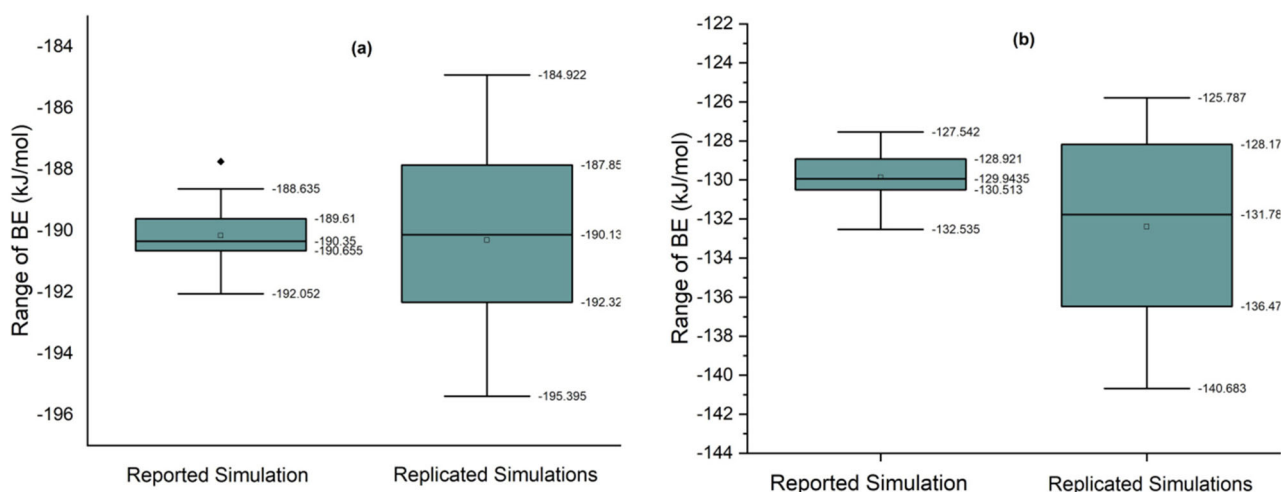
Figure 10. Box and Whisker plots that represent range of MM-PBSA binding energies obtained from 20 sets of calculations of reported and replicated simulation of (a) Amentoflavone complex and (b) Naringin complex.

Table 3. Statistical data of MM-PBSA binding energy and individual components calculated from 20 set calculations of Reported and Replicated Simulations. The standard deviation of all individual energies lies within 9 kJ/mol and 10 kJ/mol for Amentoflavone and Naringin respectively.

	Reported		Replicated	
Energy Values (kJ/mol)	Mean (kJ/mol)	Standard Deviation	Mean (kJ/mol)	Standard Deviation
Amentoflavone				
BE	−190.161	1.045	−190.305	3.105
vdW	−253.821	2.186	−246.892	5.530
ESE	−51.907	2.79	−69.851	5.159
PSE	138.862	3.367	150.537	6.283
SASA-E	−23.294	0.323	−24.096	0.726
Naringin				
BE	−129.873	1.319	−132.402	4.578
vdW	−225.155	11.624	−215.497	13.998
ESE	−54.82	15.007	−57.8	19.861
PSE	174.745	17.687	165.787	16.076
SASA-E	−24.644	1.092	−23.624	1.221

reported and replicated simulations, we finalized the mostly contributed hot spot residues that facilitate binding in the Amentoflavone-M^pro complex. The key residues that have consistent interactions throughout the simulations are found to be MET165 (-10.4), GLN189 (-7.2), MET49(-7.16), GLN192(-5.6), and HIS41(-5.2). The nature of interactions of GLN and HIS residues with Amentoflavone are observed as hydrogen bonding as well as hydrophobic-vdW type. The identified hot spot MET residues might interact with Amentoflavone through hydrophobic interactions confirmed from its nonpolar nature and the absence of any hydrogen bond. However, in the Naringin complex, consistent interaction is less. Meanwhile, more residues of M^pro contributed with small negative binding energies are observed. The MET165 is again identified as the top hot spot residue here with an energy contribution of −7.52 kJ/mol. The other amino acid residues GLN189, GLN192, and MET49 are identified as contributing residues of the Naringin complex in the reported simulation (Figure 8b) is also appeared in replicated simulation. The non-bonding interactions of MET165 residue with Amentoflavone and Naringin highlighted in the docking results (Figure 2) were also hydrophobic. A very few residues with unfavorable interactions are also observed, especially in the Naringin complex. Even though GLU166 has significant

hydrogen bonding interactions with Amentoflavone, the residue was observed as a bad contact residue (Energy contribution 3.78 kJ/mol) in the Naringin complex with unfavorable interactions. The hot spot residues may differ with the nature of ligands bind to the same target protein even though some common hot spot residues may exist for all ligands (Zoete et al., 2010).

These MM-PBSA results proposed that hydrophobic interactions and hydrogen-bonding interactions govern the binding of ligands to residues of M^pro. For better prediction, we compared the results with the recent work of Wang (Wang, 2020) focused on MM-PBSA binding energy calculations of repurposing drugs against M^pro. Interestingly, the significant binding site residues MET165, HIS41, MET49, GLN189, and GLU166, identified from our studies, are the same as reported by Wang for most ligands. Moreover, Amentoflavone (BE= −190.5 kJ/mol) and Naringin (BE=-129.87 kJ/mol) were found to be far better inhibitors of SARS-CoV-2 than all reported repurposing drugs with a maximum BE of 61.086 kJ/mol for the drug DB03147 (Wang, 2020). This is a crucial lead obtained from our MM-PBSA calculation, and the study strongly supports the inhibitory activity of Naringin and Amentoflavone. Moreover, the trend associated with the binding affinity of ligands to M^pro
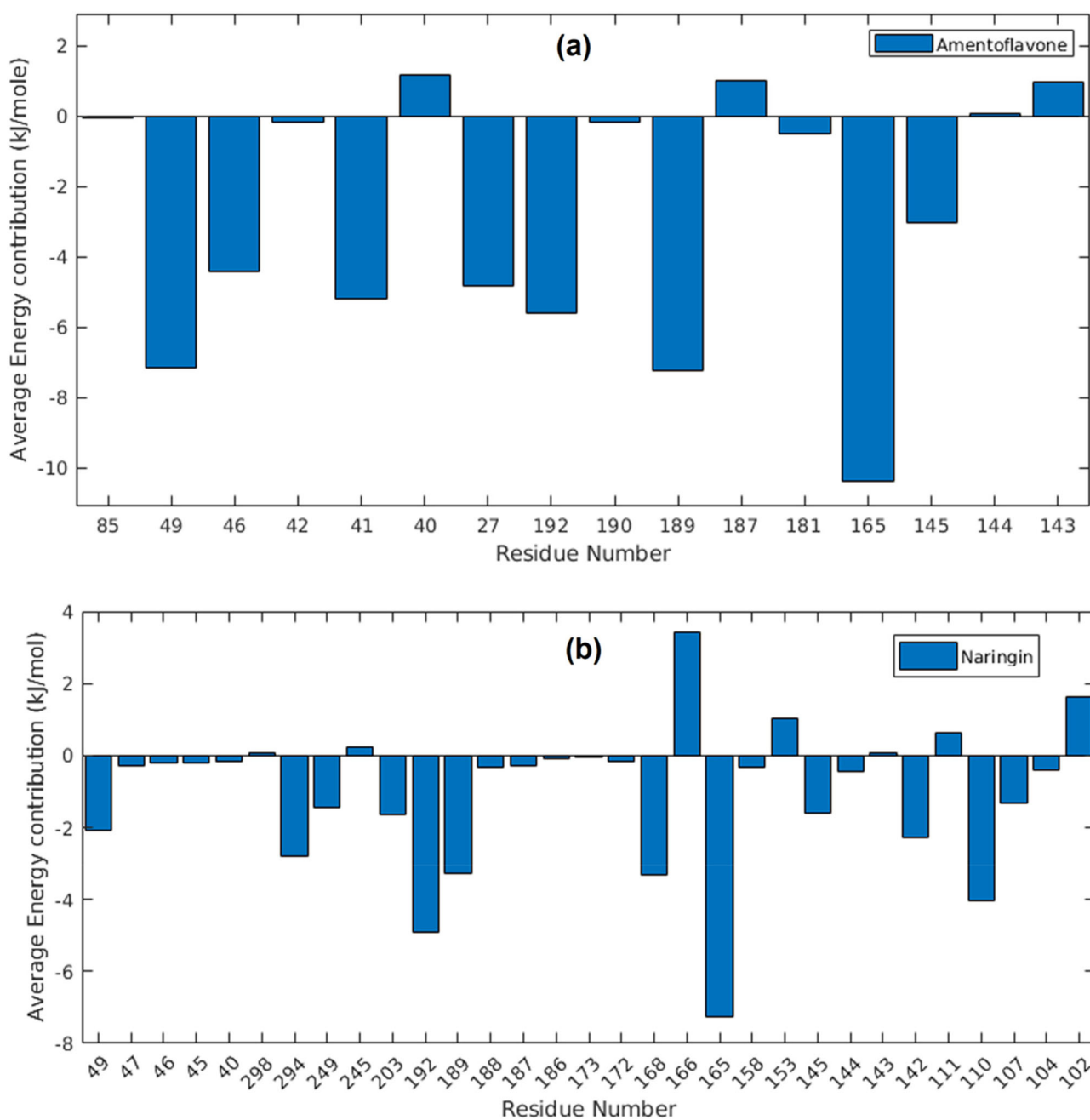
Figure 11. Average MM-PBSA binding energy contribution of residues of M^pro in the replicated simulations of (a) Amentoflavone complex and (b) Naringin complex.

obtained from the docking calculations is reproduced in the MM-PBSA calculations.

3.7. DFT binding energy calculations

The results of gaseous phase B3LYP/SVP binding energy calculations between ligand and hydrogen-bonded residues in the finite active site molecular clusters are summarized in Table 4 and Figure 12. The calculations give us an approximate estimate of hydrogen bond energy and binding interactions based on the electronic structure of the ligand and the residues. The hydrogen bond pairs in the current calculation can be denoted as D-H-A, where D and A are donor

Table 4. Binding energy of ligands obtained obtained from DFT calculations.

Ligand	E[(RES-LIG) (Ha)]	E(RES) (Ha)	E(LIG) (Ha)	BE (kJ/mole)
Amentoflavone	−3500.00	−1594.83	−1905.1	−182.92
Naringin	−3236.35	−1137.71	−2098.58	−160.67

(highlighted with pink color) and acceptor (highlighted with green color) atoms of protein or ligand residues, respectively.

The donor-acceptor pairs of hydrogen bonds associated with Amentoflavone under investigation are LIG307@O-CYS44@O, LIG307@O-HIS41@(ND1/NE2), and GLU166@N-LIG307@O, respectively. In the case of Naringin, the pairs are GLY143@N-LIG307@O, GLN192@OE1-LIG307@O, and HIS163@NE2-LIG307@O respectively. It is observed that
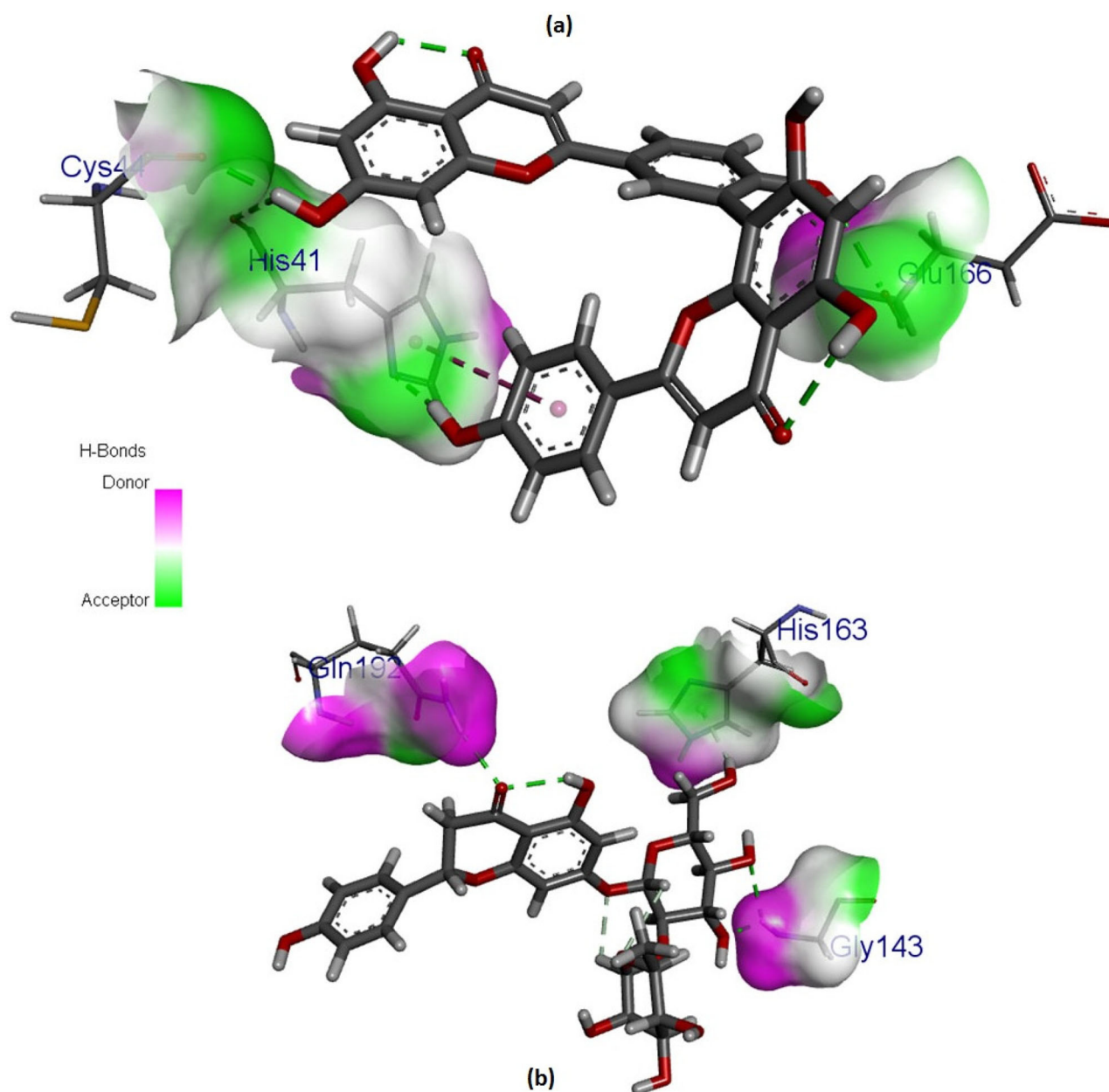
Figure 12. Active Site Molecular clusters used in DFT binding energy calculations of (a) Amentoflavone and (b) Naringin with hydrogen bonded residues.

atoms of Naringin act as hydrogen bond donors, and that of Amentoflavone act as acceptors in most cases. A comparison of binding energy is possible since equal numbers of hydrogen bond pairs are associated with both ligands. In this competitive binding, Amentoflavone is identified as a better binder with energy of −182.92 kJ/mol compared to Naringin (-160.67 kJ/mol). The negative binding energy with a higher magnitude for Amentoflavone and Naringin indicates stable protein-ligand complex formation. Once again, the trends of binding affinity of Amentoflavone and Naringin to M^{pro} are repeated in the electronic structure calculations.

4. Conclusion

It will be highly beneficial if natural compounds can be used as pharmacological agents without the fear of side effects to reduce and prevent the spread of COVID-19, which is currently a big concern for global public health. Identification of the natural dietary compounds that may be useful for home care of COVID– 19 patients is the key focus of this work. We identified various dietary compounds like Naringin, Amentoflavone, and Naringenin that are inhibitors against SARS-CoV-2 protease in terms of binding affinity. Our results showed that Naringin and Amentoflavone fit well into the active site of the protein with better binding energy. Hydrophobic and hydrogen bond interactions are the key mechanism in the binding of these ligands with the active site residues. We predict that Amentoflavone has dominant inhibitory activity than Naringin from the results obtained from docking, hydrogen bond occupancy analysis, MM-PBSA, and DFT calculations. This study also recognizes some of the key amino acid residues MET165, HIS41, CYS145, GLU166, GLY143, SER144, HIS163, PRO168, GLN189, GLN192, ASN142, and MET49 of M^{pro} that may involve in the interaction with potential inhibitors. To the best of our knowledge,

Amentoflavone and Naringin, widely available nutritional supplements, are introduced for the first time as a potential inhibitor of SARS-CoV-2 that may act as a lead compound for drug development against COVID-19.

Associated content

We provide the following files and data in the supporting file (a) Table with docking scores of different flavonoids against M^{pro} (b) Cartesian Coordinates of Molecules used in docking and DFT calculations) Autodock 4.2.6 Results (d) Ramachandran plot analysis (e) Results of Twenty sets of MM-PBSA Calculations from reported and replicated simulations (f) MM-PBSA residue decomposition of Naringenin Complex (g) movie of MD simulation of Naringin and Amentoflavone Complex in water highlighting protein-ligand interactions.

Disclosure statement

No potential conflict of interest was reported by the author(s).

ORCID

K. S. Sindhu 🆔 http://orcid.org/0000-0003-1392-3974
T. G. Abi 🆔 http://orcid.org/0000-0002-5915-8609

References

Ahmad, A., Kaleem, M., Ahmed, Z., & Shafiq, H. (2015). Therapeutic potential of flavonoids and their mechanism of action against microbial and viral infections—A review. *Food Research International*, 77, 221–235. https://doi.org/10.1016/j.foodres.2015.06.021

Bauernschmitt, R., Häser, M., Treutler, O., & Ahlrichs, R. (1997). Calculation of excitation energies within time-dependent density functional theory using auxiliary basis set expansions. *Chemical Physics Letters*, 264(6), 573–578. https://doi.org/10.1016/S0009-2614(96)01343-7

Becke, A. D. (1988). Density-functional exchange-energy approximation with correct asymptotic behavior. *Physical Review. A, General Physics*, 38(6), 3098–3100. https://doi.org/10.1103/physreva.38.3098

Berendsen, H. J. C., Postma, J. P. M., Gunsteren, WFv., DiNola, A., & Haak, J. R. (1984). Molecular dynamics with coupling to an external bath. *The Journal of Chemical Physics*, 81(8), 3684–3690. https://doi.org/10.1063/1.448118

Berendsen, H. J. C., van der Spoel, D., & van Drunen, R. (1995). GROMACS: A message-passing parallel molecular dynamics implementation. *Computer Physics Communications*, 91(1-3), 43–56. https://doi.org/10.1016/0010-4655(95)00042-E

Caly, L., Druce, J. D., Catton, M. G., Jans, D. A., & Wagstaff, K. M. (2020). The FDA-approved drug ivermectin inhibits the replication of SARS-CoV-2 in vitro. *Antiviral Research*, 178, 104787 https://doi.org/10.1016/j.antiviral.2020.104787

Chan, J. F.-W., Kok, K.-H., Zhu, Z., Chu, H., To, K. K.-W., Yuan, S., & Yuen, K.-Y. (2020). Genomic characterization of the 2019 novel human-pathogenic coronavirus isolated from a patient with atypical pneumonia after visiting Wuhan. *Emerging Microbes & Infections*, 9(1), 221–236. https://doi.org/10.1080/22221751.2020.1719902

Chen, R., Qi, Q. L., Wang, M. T., & Li, Q. Y. (2016). Therapeutic potential of naringin: An overview. *Pharmaceutical Biology*, 54(12), 3203–3210. Epub 2016/08/27. https://doi.org/10.1080/13880209.2016.1216131

Chu, C. M., Cheng, V. C. C., Hung, I. F. N., Wong, M. M. L., Chan, K. H., Chan, K. S., Kao, R. Y. T., Poon, L. L. M., Wong, C. L. P., Guan, Y., Peiris, J. S. M., Yuen, K. Y., & Group, H. U. S. S. (2004). Role of lopinavir/ritonavir in the treatment of SARS: Initial virological and clinical findings. *Thorax*, 59(3), 252–256. https://doi.org/10.1136/thorax.2003.012658

Cortegiani, A., Ippolito, M., Greco, M., Granone, V., Protti, A., Gregoretti, C., Giarratano, A., Einav, S., & Cecconi, M. (2021). Rationale and evidence on the use of tocilizumab in COVID-19: A systematic review. *Pulmonology*, 27(1), 52–66. https://doi.org/10.1016/j.pulmoe.2020.07.003

Dai, W., Bi, J., Li, F., Wang, S., Huang, X., Meng, X., Sun, B., Wang, D., Kong, W., Jiang, C., & Su, W. (2019). Antiviral Efficacy of Flavonoids against Enterovirus 71 Infection in Vitro and in Newborn Mice. *Viruses*, 11(7), 625. https://doi.org/10.3390/v11070625

Dai, W., Zhang, B., Jiang, X.-M., Su, H., Li, J., Zhao, Y., Xie, X., Jin, Z., Peng, J., Liu, F., Li, C., Li, Y., Bai, F., Wang, H., Cheng, X., Cen, X., Hu, S., Yang, X., Wang, J., … Liu, H. (2020). Structure-based design of antiviral drug candidates targeting the SARS-CoV-2 main protease. *Science (New York, N.Y.)*, 368(6497), 1331–1335. https://doi.org/10.1126/science.abb4489

Di Pierro, M., Elber, R., & Leimkuhler, B. (2015). A Stochastic Algorithm for the isobaric-isothermal ensemble with Ewald summations for all long range forces. *Journal of Chemical Theory and Computation*, 11(12), 5624–5637. https://doi.org/10.1021/acs.jctc.5b00648

Dietary Bioactive Components. (2018). Current Developments in Nutrition (2018). 2.

Dodda, L. S., Cabeza de Vaca, I., Tirado-Rives, J., & Jorgensen, W. L. (2017). LigParGen web server: An automatic OPLS-AA parameter generator for organic ligands. *Nucleic Acids Research*, 45(W1), W331–W6. https://doi.org/10.1093/nar/gkx312

Ferreira de Freitas, R., & Schapira, M. (2017). A systematic analysis of atomic protein-ligand interactions in the PDB. *MedChemComm*, 8(10), 1970–1981. https://doi.org/10.1039/c7md00381a

Frecer, V., & Miertus, S. (2020). Antiviral agents against COVID-19: Structure-based design of specific peptidomimetic inhibitors of SARS-CoV-2 main protease. *RSC Advances*, 10(66), 40244–40263. https://doi.org/10.1039/D0RA08304F

Gandhi, R. T., Lynch, J. B., & del Rio, C. (2020). Mild or Moderate Covid-19. *New England Journal of Medicine*, 383(18), 1757–1766. https://doi.org/10.1056/NEJMcp2009249

Genheden, S., & Ryde, U. (2015). The MM/PBSA and MM/GBSA methods to estimate ligand-binding affinities. *Expert Opinion on Drug Discovery*, 10(5), 449–461. Epub 2015/04/04. https://doi.org/10.1517/17460441.2015.1032936

Ghosh, R., Chakraborty, A., Biswas, A., & Chowdhuri, S. (2020). Evaluation of green tea polyphenols as novel corona virus (SARS CoV-2) main protease (Mpro) inhibitors – an in silico docking and molecular dynamics simulation study. *Journal of Biomolecular Structure and Dynamics*, 1–13.

Ghosh, R., Chakraborty, A., Biswas, A., & Chowdhuri, S. (2020). Identification of polyphenols from Broussonetia papyrifera as SARS CoV-2 main protease inhibitors using in silico docking and molecular dynamics simulation approaches. *Journal of Biomolecular Structure and Dynamics*, 1–14.

Gogoi, N., Chowdhury, P., Goswami, A. K., Das, A., Chetia, D., & Gogoi, B. (2020). Computational guided identification of a citrus flavonoid as potential inhibitor of SARS-CoV-2 main protease. *Molecular Diversity*.

Grein, J., Ohmagari, N., Shin, D., Diaz, G., Asperges, E., Castagna, A., Feldt, T., Green, G., Green, M. L., Lescure, F.-X., Nicastri, E., Oda, R., Yo, K., Quiros-Roldan, E., Studemeister, A., Redinski, J., Ahmed, S., Bernett, J., Chelliah, D., … Flanigan, T. (2020). Compassionate Use of Remdesivir

for Patients with Severe Covid-19. *New England Journal of Medicine*, *382*(24), 2327–2336. https://doi.org/10.1056/NEJMoa2007016

Hou, Q., & Zhang, L. (2020). Biomimetic Design of Peptide Neutralizer of Ebola Virus with Molecular Simulation. *Langmuir : The ACS Journal of Surfaces and Colloids*, *36*(7), 1813–1821. https://doi.org/10.1021/acs.langmuir.9b03832

Ibrahim, M. A. A., Abdelrahman, A. H. M., Hussien, T. A., Badr, E. A. A., Mohamed, T. A., El-Seedi, H. R., Pare, P. W., Efferth, T., & Hegazy, M. F. (2020). In silico drug discovery of major metabolites from spices as SARS-CoV-2 main protease inhibitors. *Computers in Biology and Medicine*, *126*, 104046Epub 2020/10/17. https://doi.org/10.1016/j.compbiomed.2020.104046

Idrees, M., Khan, S., Memon, N. H., & Zhang, Z. (2020). Effect of the Phytochemical Agents Against the SARS-CoV and Selected Some of them for Application to COVID-19: A Mini-Review. *Current Pharmaceutical Biotechnology*, *21* Epub 2020/07/04. https://doi.org/10.2174/1389201021666200703201458

Iwata-Yoshikawa, N., Okamura, T., Shimizu, Y., Hasegawa, H., & Takeda, M. (2019). TMPRSS2 Contributes to Virus Spread and Immunopathology in the Airways of Murine Models after Coronavirus Infection, 93.

Jin, Z., Du, X., Xu, Y., Deng, Y., Liu, M., Zhao, Y., Zhang, B., Li, X., Zhang, L., Peng, C., Duan, Y., Yu, J., Wang, L., Yang, K., Liu, F., Jiang, R., Yang, X., You, T., Liu, X., … Yang, H. (2020). Structure of Mpro from SARS-CoV-2 and discovery of its inhibitors. *Nature*, *582*(7811), 289–293. https://doi.org/10.1038/s41586-020-2223-y

Jin, Z., Zhao, Y., Sun, Y., Zhang, B., Wang, H., Wu, Y., Zhu, Y., Zhu, C., Hu, T., Du, X., Duan, Y., Yu, J., Yang, X., Yang, X., Yang, K., Liu, X., Guddat, L. W., Xiao, G., Zhang, L., Yang, H., & Rao, Z. (2020). Structural basis for the inhibition of SARS-CoV-2 main protease by antineoplastic drug carmofur. *Nat Struct Mol Biol*, *27*(6), 529–532. https://doi.org/10.1038/s41594-020-0440-6

Jomah, S., Asdaq, S. M. B., & Al-Yamani, M. J. (2020). Clinical efficacy of antivirals against novel coronavirus (COVID-19): A review. *J Infect Public Health*, *13*(9), 1187–1195. https://doi.org/10.1016/j.jiph.2020.07.013

Jorgensen, W. L., Maxwell, D. S., & Tirado-Rives, J. (1996). Development and Testing of the OPLS All-Atom Force Field on Conformational Energetics and Properties of Organic Liquids. *Journal of the American Chemical Society*, *118*(45), 11225–11236. https://doi.org/10.1021/ja9621760

Joshi, R. S., Jagdale, S. S., Bansode, S. B., Shankar, S. S., Tellis, M. B., Pandya, V. K., Chugh, A., Giri, A. P., & Kulkarni, M. J. (2020). Discovery of potential multi-target-directed ligands by targeting host-specific SARS-CoV-2 structurally conserved main protease. *Journal of Biomolecular Structure and Dynamics*, 1–16.

Kabsch, W., & Sander, C. (1983). Dictionary of protein secondary structure: Pattern recognition of hydrogen-bonded and geometrical features. *Biopolymers*, *22*(12), 2577–2637. Epub 1983/12/01. https://doi.org/10.1002/bip.360221211

Kollman, P. A., Massova, I., Reyes, C., Kuhn, B., Huo, S., Chong, L., Lee, M., Lee, T., Duan, Y., Wang, W., Donini, O., Cieplak, P., Srinivasan, J., Case, D. A., & Cheatham, T. E. (2000). Calculating Structures and Free Energies of Complex Molecules: Combining Molecular Mechanics and Continuum models. *Accounts of Chemical Research*, *33*(12), 889–897. https://doi.org/10.1021/ar000033j

Kumar, Y., Singh, H., & Patel, C. N. (2020). In silico prediction of potential inhibitors for the main protease of SARS-CoV-2 using molecular docking and dynamics simulation based drug-repurposing. *Journal of Infection and Public Health*, *13*(9), 1210–1223. https://doi.org/10.1016/j.jiph.2020.06.016

Kumari, R., Kumar, R., & Lynn, A. (2014). g_mmpbsa-a GROMACS tool for high-throughput MM-PBSA calculations . *Journal of Chemical Information and Modeling*, *54*(7), 1951–1962. https://doi.org/10.1021/ci500020m

Li, W., Moore, M. J., Vasilieva, N., Sui, J., Wong, S. K., Berne, M. A., Somasundaran, M., Sullivan, J. L., Luzuriaga, K., Greenough, T. C., Choe, H., & Farzan, M. (2003). Angiotensin-converting enzyme 2 is a functional receptor for the SARS coronavirus. *Nature*, *426*(6965), 450–454. Epub 2003/12/04. https://doi.org/10.1038/nature02145

Li, F., Song, X., Su, G., Wang, Y., Wang, Z., Jia, J., Qing, S., Huang, L., Wang, Y., Zheng, K., & Wang, Y. (2019). Amentoflavone Inhibits HSV-1 and ACV-Resistant Strain Infection by Suppressing Viral Early Infection. *Viruses*, *11*(5), 466. https://doi.org/10.3390/v11050466

Li, S., Xu, W., Chu, S., Ma, N., Liu, S., Li, X., Wang, T., Jiang, X., Li, F., Li, Y., Zhang, D., Luo, Q., & Liu, J. (2019). Computational Design and Study of Artificial Selenoenzyme with Controllable Activity Based on an Allosteric Protein Scaffold. *Chemistry (Weinheim an Der Bergstrasse, Germany)*, *25*(44), 10350–10358. https://doi.org/10.1002/chem.201901480

Liu, R. H. (2013). Dietary Bioactive Compounds and Their Health Implications. *Journal of Food Science*, *78*(s1), A18–A25. https://doi.org/10.1111/1750-3841.12101

Mani, J. S., Johnson, J. B., Steel, J. C., Broszczak, D. A., Neilsen, P. M., Walsh, K. B., & Naiker, M. (2020). Natural product-derived phytochemicals as potential agents against coronaviruses: A review. *Virus Res*, *284*, 197989 https://doi.org/10.1016/j.virusres.2020.197989

Middleton, E., Kandaswami, C., & Theoharides, T. C. (2000). The Effects of Plant Flavonoids on Mammalian Cells: Implications for Inflammation, Heart Disease, and Cancer. *Pharmacological Reviews*, *52*(4), 673–751.

Moghaddam, E., Teoh, B.-T., Sam, S.-S., Lani, R., Hassandarvish, P., Chik, Z., Yueh, A., Abubakar, S., & Zandi, K. (2014). Baicalin, a metabolite of baicalein with antiviral activity against dengue virus. *Scientific Reports*, *4*, 5452 https://doi.org/10.1038/srep05452

Muhseen, Z. T., Hameed, A. R., Al-Hasani, H. M. H., Tahir Ul Qamar, M., & Li, G. (2020). Promising terpenes as SARS-CoV-2 spike receptor-binding domain (RBD) attachment inhibitors to the human ACE2 receptor: Integrated computational approach. *J Mol Liq*, *320*, 114493 https://doi.org/10.1016/j.molliq.2020.114493

Richardson, P., Griffin, I., Tucker, C., Smith, D., Oechsle, O., Phelan, A., Rawling, M., Savory, E., & Stebbing, J. (2020). Baricitinib as potential treatment for 2019-nCoV acute respiratory disease. *The Lancet*, *395*(10223), e30–e1. https://doi.org/10.1016/S0140-6736(20)30304-4

Ryu, Y. B., Jeong, H. J., Kim, J. H., Kim, Y. M., Park, J.-Y., Kim, D., Nguyen, T. T. H., Park, S.-J., Chang, J. S., Park, K. H., Rho, M.-C., & Lee, W. S. (2010). Biflavonoids from Torreya nucifera displaying SARS-CoV 3CL(pro) inhibition. *Bioorganic & Medicinal Chemistry*, *18*(22), 7940–7947. https://doi.org/10.1016/j.bmc.2010.09.035

Saha, R. P., Sharma, A. R., Singh, M. K., Samanta, S., Bhakta, S., Mandal, S., Bhattacharya, M., Lee, S.-S., & Chakraborty, C. (2020). Repurposing Drugs, Ongoing Vaccine, and New Therapeutic Development Initiatives Against COVID-19. *Frontiers in Pharmacology*, *11*, 1258. https://doi.org/10.3389/fphar.2020.01258

Salehi, B., Fokou, P. V. T., Sharifi-Rad, M., Zucca, P., Pezzani, R., Martins, N., & Sharifi-Rad, J. (2019). The Therapeutic Potential of Naringenin: A Review of Clinical Trials. *Pharmaceuticals*, *12*(1), 11. https://doi.org/10.3390/ph12010011

Salentin, S., Schreiber, S., Haupt, V. J., Adasme, M. F., & Schroeder, M. (2015). PLIP: Fully automated protein-ligand interaction profiler. *Nucleic Acids Research*, *43*(W1), W443–W7. Epub 04/14. https://doi.org/10.1093/nar/gkv315

Scalbert, A., Manach, C., Morand, C., Rémésy, C., & Jiménez, L. (2005). Dietary Polyphenols and the Prevention of Diseases. *Crit Rev Food Sci Nutr*, *45*(4), 287–306. https://doi.org/10.1080/1040869059096

Schäfer, A., Horn, H., & Ahlrichs, R. (1992). Fully optimized contracted Gaussian basis sets for atoms Li to Kr. *The Journal of Chemical Physics*, *97*(4), 2571–2577. https://doi.org/10.1063/1.463096

Schoeman, D., & Fielding, B. C. (2019). Coronavirus envelope protein: Current knowledge. *Virology Journal*, *16*(1), 69 https://doi.org/10.1186/s12985-019-1182-0

Singh, A., & Mishra, A. (2020). Leucoefdin a potential inhibitor against SARS CoV-2 Mpro. *Journal of Biomolecular Structure and Dynamics*, 1–6.

Toukan, K., & Rahman, A. (1985). Molecular-dynamics study of atomic motions in water. *Physical Review. B, Condensed Matter*, *31*(5), 2643–2648. https://doi.org/10.1103/physrevb.31.2643

Trott, O., & Olson, A. J. (2010). AutoDock Vina: Improving the speed and accuracy of docking with a new scoring function, efficient optimization, and multithreading. *Journal of Computational Chemistry*, *31*(2), 455–461. https://doi.org/10.1002/jcc.21334

Umesh, K. D., Selvaraj, C., Singh, S. K., & Dubey, V. K. (2020). Identification of new anti-nCoV drug chemical compounds from Indian spices exploiting SARS-CoV-2 main protease as target. *Journal of Biomolecular Structure & Dynamics*, 1–9. Epub 2020/05/05.

Wang, J. (2020). Fast Identification of Possible Drug Treatment of Coronavirus Disease-19 (COVID-19) through Computational Drug Repurposing Study. *Journal of Chemical Information and Modeling*, *60*(6), 3277–3286. https://doi.org/10.1021/acs.jcim.0c00179

Wang, E., Sun, H., Wang, J., Wang, Z., Liu, H., Zhang, J. Z. H., & Hou, T. (2019). End-Point Binding Free Energy Calculation with MM/PBSA and MM/GBSA: Strategies and Applications in Drug Design. *Chemical Reviews*, *119*(16), 9478–9508. https://doi.org/10.1021/acs.chemrev.9b00055

Wu, Y.-C., Chen, C.-S., & Chan, Y.-J. (2020). The outbreak of COVID-19: An overview. *Journal of the Chinese Medical Association: JCMA*, *83*(3), 217–220. https://doi.org/10.1097/JCMA.0000000000000270

Yao, X., Ye, F., Zhang, M., Cui, C., Huang, B., Niu, P., Liu, X., Zhao, L., Dong, E., Song, C., Zhan, S., Lu, R., Li, H., Tan, W., & Liu, D. (2020). In Vitro Antiviral Activity and Projection of Optimized Dosing Design of Hydroxychloroquine for the Treatment of Severe Acute Respiratory Syndrome Coronavirus 2 (SARS-CoV-2. *Clinical Infectious Diseases : An Official Publication of the Infectious Diseases Society of America*, *71*(15), 732–739.). https://doi.org/10.1093/cid/ciaa237

Zhang, J., Ma, X., Yu, F., Liu, J., Zou, F., Pan, T., & Zhang, H. Teicoplanin potently blocks the cell entry of 2019-nCoV. bioRxiv; (2020).

Zhou, P., Yang, X.-L., Wang, X.-G., Hu, B., Zhang, L., Zhang, W., Si, H.-R., Zhu, Y., Li, B., Huang, C.-L., Chen, H.-D., Chen, J., Luo, Y., Guo, H., Jiang, R.-D., Liu, M.-Q., Chen, Y., Shen, X.-R., Wang, X., … Shi, Z.-L. (2020). A pneumonia outbreak associated with a new coronavirus of probable bat origin. *Nature*, *579*(7798), 270–273. https://doi.org/10.1038/s41586-020-2012-7

Zoete, V., Irving, M. B., & Michielin, O. (2010). MM-GBSA binding free energy decomposition and T cell receptor engineering. *Journal of Molecular Recognition : JMR*, *23*(2), 142–152. https://doi.org/10.1002/jmr.1005